**Zhenguo Nie**
Beijing Key Lab of Precision/Ultra-Precision Manufacturing Equipments and Control, Tsinghua University, Beijing 100084, China;
George W. Woodruff School of Mechanical Engineering, Georgia Institute of Technology, Atlanta, GA 30332-0405
e-mails: zhenguo.nie@me.gatech.edu; zhenguonie@gmail.com

**Gang Wang**[1]
Beijing Key Lab of Precision/Ultra-Precision Manufacturing Equipments and Control, Tsinghua University, Beijing 100084, China;
Department of Mechanical Engineering, Tsinghua University, Beijing 100084, China
e-mail: gwang@tsinghua.edu.cn

**Dehao Liu**
Beijing Key Lab of Precision/Ultra-Precision Manufacturing Equipments and Control, Tsinghua University, Beijing 100084, China;
George W. Woodruff School of Mechanical Engineering, Georgia Institute of Technology, Atlanta, GA 30332-0405

**Yiming (Kevin) Rong**
Beijing Key Lab of Precision/Ultra-Precision Manufacturing Equipments and Control, Tsinghua University, Beijing 100084, China;
Department of Mechanical and Energy Engineering, South University of Science and Technology of China, Shenzhen 518055, China

# A Statistical Model of Equivalent Grinding Heat Source Based on Random Distributed Grains

*Accurate information about the evolution of the temperature field is a theoretical prerequisite for investigating grinding burn and optimizing the process parameters of grinding process. This paper proposed a new statistical model of equivalent grinding heat source with consideration of the random distribution of grains. Based on the definition of the Riemann integral, the summation limit of the discrete point heat sources was transformed into the integral of a continuous function. A finite element method (FEM) simulation was conducted to predict the grinding temperature field with the embedded net heat flux equation. The grinding temperature was measured with a specially designed in situ infrared system and was formulated by time–space processing. The reliability and correctness of the statistical heat source model were validated by both experimental temperature–time curves and the maximum grinding temperature, with a relative error of less than 20%. Finally, through the FEM-based inversed calculation, an empirical equation was proposed to describe the heat transfer coefficient (HTC) changes in the grinding contact zone for both conventional grinding and creep feed grinding.* [DOI: 10.1115/1.4038729]

*Keywords: statistical model, grinding temperature field, heat flux distribution, grinding temperature measurement, empirical equation of HTC*

## 1 Introduction

Grinding is commonly used as the final machining process to obtain a high-quality surface with low roughness and tolerance. Compared with other machining processes, grinding generates more thermal energy and has a high temperature and temperature gradient. As shown in Fig. 1, grinding burn occurs in creep feed grinding of last stage rotating blades. In the creep feed grinding of blade fir-tree root, the cutting depth was 0.3 mm, the linear speed of wheel was 20 m/s, and the feed rate of workpiece was 80 mm/min. The specific grinding energy can reach 100–300 J/mm$^2$. High grinding temperature induces surface oxidation, phase transformation, thermal cracking, and residual stress; therefore, research on the temperature field during the grinding process is important. Optimization of the grinding process requires good knowledge of the heat flux input and maximum temperature increase [1]. For this reason, precise prediction of the grinding temperature field is a basic requirement in the analysis and prevention of thermal damage.

The heat flux distribution is a critical factor for precise result acquisition. Several empirical heat flux models have been used in finite element method (FEM) simulation in past decades, such as rectangular heat flux [2,3], triangular heat flux [1,4], and parabolic heat flux [5]. The empirical models usually require experimental temperature data to support and deduce some of the heat flux parameters, so it is difficult to predict the grinding temperature

Fig. 1 Grinding burn on the surface of turbine blade fir-tree root after creep feed grinding

[1]Corresponding author.

Manuscript received September 13, 2017; final manuscript received December 4, 2017; published online March 7, 2018. Assoc. Editor: Y. B. Guo.

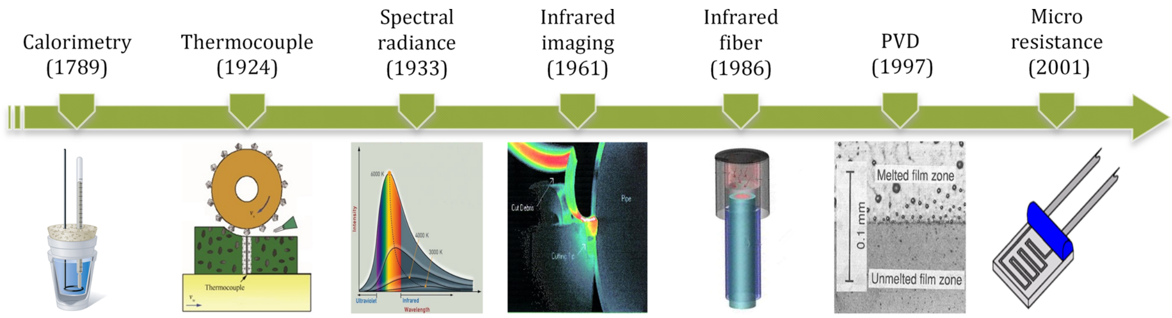


**Fig. 2 Development history of temperature measurement in machining: calorimetry [9], thermocouple [10], spectral radiance [11], infrared imaging [12], infrared optical fiber [13], PVD [14], and micro resistance [15]**

without temperature measurement. Theoretical heat flux models based on thermal analysis of the distribution ratio were proposed for precise modeling [6,7], and all current theoretical models are based on the theory that the heat flux input is an integral on a continuous contact surface without discrete grains. Many of the model parameters remain uncertain and are difficult to determine. The Monte Carlo method is an alternative way to simulate the grinding temperature field [8]. It was established that the temperature field has a quasi-stationary occasional character. Therefore, the calculated result cannot predict the real grinding temperature field, and only the stabilization zone conformed to the constant level of temperature field formation.

With the development of temperature measurement technology, various methods have been applied in machining processes to assess temperature variation. Figure 2 shows the development history of temperature measurement methods in machining processes.

In contrast to other machining processes, grinding temperature measurement has a challenging problem of measuring reachability. Scholars have considered many measurement methods, such as thermocouples, infrared radiation pyrometers, infrared imaging systems, and the physical vapor deposition (PVD) film method, to obtain accurate and reliable results. Thermocouples are the most commonly used thermometers in machining processes and can be applied in various methods, including embedded style (double pole) [16–18] and foil/workpiece style (single pole) [5]. Thermocouples have the advantages of rapid response, high precision, and good durability; however, they are easily influenced by mechanical vibration and external electromagnetic conditions during the grinding process. Infrared radiation pyrometers with optical fibers [16,19–21] trap the infrared rays radiated from the grinding zone to calculate the maximum temperature via the Stefan–Boltzmann law. The disadvantage of infrared radiation pyrometers is that the device cannot measure the temperature field, only the maximum value. Infrared imaging systems [20,22] are an effective way to obtain the grinding temperature field by monitoring the workpiece profile. However, the maximum temperature is difficult to measure owing to the obstructing effect of the abrasive wheel. The PVD film method [14] is another feasible method to obtain the isothermal curves of a workpiece. In the PVD film method, a thin film is deposited on the workpiece profile by using PVD, grinding heat melts the top part film, and an isothermal curve is plotted with the temperature of the film's melting point. The PVD method has not been used broadly owing to its large measurement error and labor-intensive process.

In this paper, a new statistical model of a grinding heat source based on the random grain distribution is proposed first. The sum of the discrete point heat flux is transformed into an integral of a continuous function via the Riemann integral. Then, the net heat flux equation is deduced and plugged into the FEM. The dynamic grinding temperature field can then be computed by finite element simulation. Second, grinding temperature fields are measured via a specially designed in situ temperature measurement system to validate the heat source model. The validation showed that the statistical heat flux model could be used to accurately predict the grinding temperature via FEM. Finally, an empirical equation is proposed to describe the heat transfer coefficient (HTC) of the grinding contact zone by FEM-based inversed calculation.

## 2 Modeling of the Equivalent Grinding Heat Source

The total grinding heat generated by friction can be transferred into five components: heat absorbed by abrasive grains, heat taken away by chips, heat convection by coolant or air, heat radiation, and heat causing a workpiece temperature increase [23].

According to the thermal flow sequence of grinding heat shown in Fig. 3, the total heat flux ($q_0$) is split into two portions: $q_g$, which goes into the grains, and $q_w$, which goes into the workpiece.

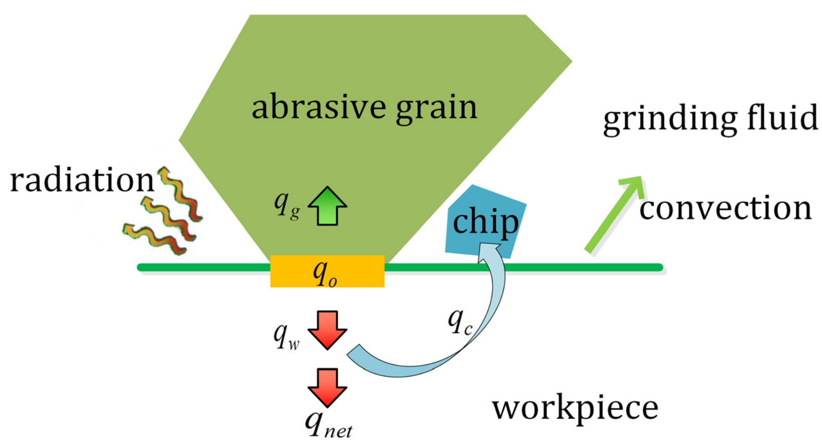


**Fig. 3 Flow directions of the grinding heat**

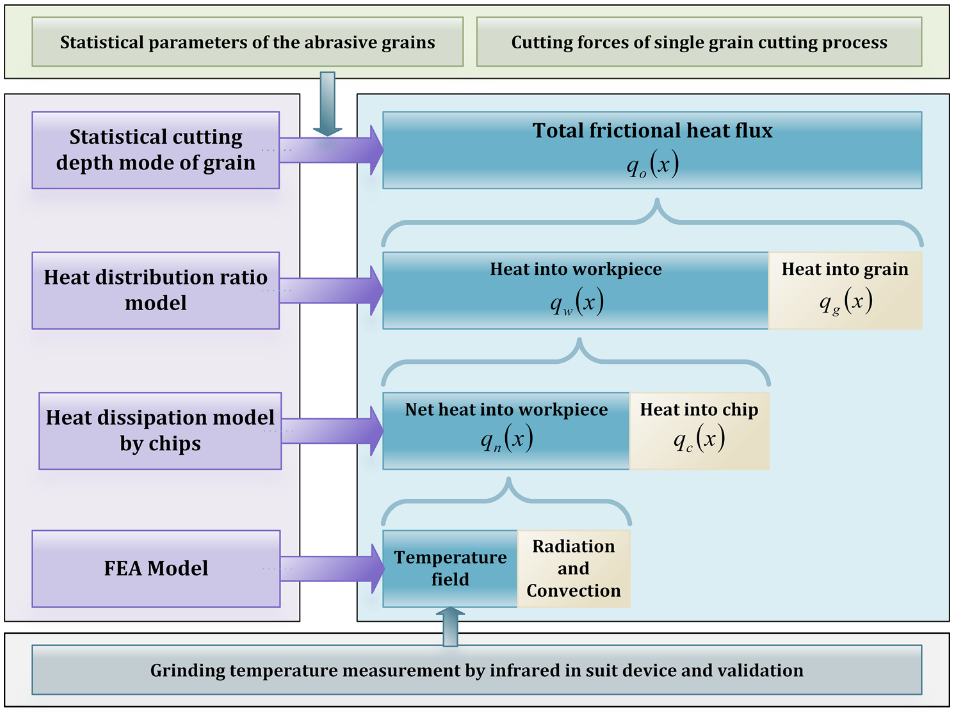


**Fig. 4 Schematic diagram of the statistical modeling method of the grinding temperature field**

Furthermore, $q_w$ consists of two portions: the heat flux taken away by chips, $q_c$, and the net heat flux causing a temperature rise in the workpiece, $q_n$. In addition, when the workpiece is heated, some of the heat is dissipated through the external surface via convection and radiation. Heat dissipated via convection and radiation is part of the net heat flux, $q_n$. Therefore, the final temperature field of a workpiece is affected by both $q_n$ and dissipation effects. The quantitative relationships are expressed in Eqs. (1) and (2)

$$q_0 = q_w + q_g \tag{1}$$

$$q_w = q_n + q_c \tag{2}$$

The schematic diagram in Fig. 4 shows the general outline of this paper. The statistical single grain cutting depth is a critical factor in the overall modeling process. The total frictional heat flux can be obtained via statistics. The statistical parameters of the abrasive grains and cutting forces of a single grain are used to support the frictional work model. Then, the heat distribution ratio between the grain and workpiece is modeled according to Hahn's theory. The heat distribution ratio clearly separates the components of the heat flux into the workpiece and grains, and the net heat flux into the workpiece is expressed by a mathematical formula based on the modeling of the heat dissipation by the grinding chips. An FEM model based on the net heat flux can provide the temperature field of workpiece. Finally, the grinding temperature is measured using a specially designed in situ system, and the experimental data are used to validate the reliability and correctness of the statistical heat source model.

**2.1 Penetration Depth of a Single Grain.** Figure 5 shows the paths of the abrasive grains passing through the grinding zone. The grains are assumed to be uniformly distributed on the abrasive wheel with the same protrusion height. The normal distance between two adjacent trajectories is called the penetration depth $h(x)$. With increasing penetration depth, the deformation of the surface material goes through three stages: sliding, plowing, and cutting. As shown in Fig. 6, the statistical penetration depth $h(x)$ at any point $P(x, y)$ can be calculated by Eq. (3) [24]

$$h(x) = \frac{2\lambda_{sl} v_w}{v_s}\sqrt{\frac{y}{d_s}} \tag{3}$$

where $\lambda_{sl}$ is the average distance between two effective front and back grains, $v_w$ is the feed rate of the workpiece, $v_s$ is the linear

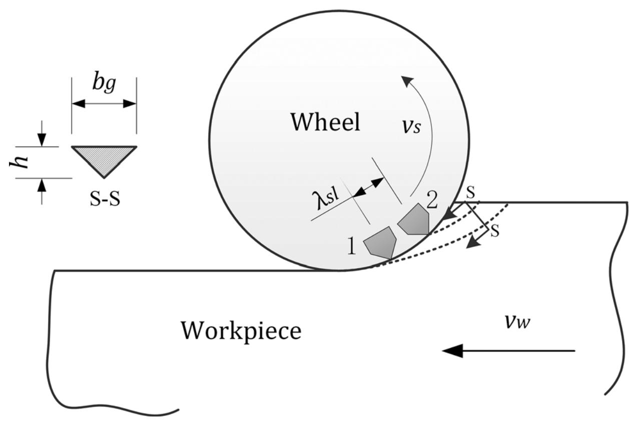


**Fig. 5 Schematic diagram of single grain grinding**

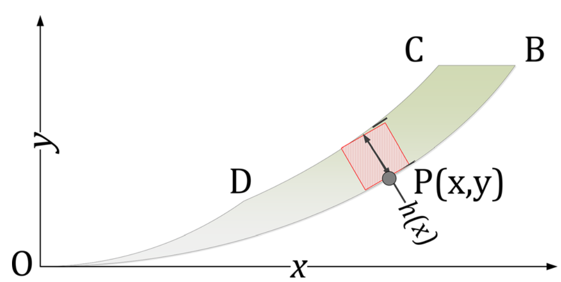


**Fig. 6 Penetration depth of a single grain**

speed of the abrasive wheel, $d_s$ is the abrasive wheel diameter, and $y$ is the grinding depth of the abrasive wheel at point $P(x, y)$.

The average distance $\lambda_{sl}$ between two effective adjacent grains is not the same as the mean scattered spacing $\bar{\lambda}_s$ of the abrasive grains. The relationship between $\lambda_{sl}$ and $\bar{\lambda}_s$ can be express in Eq. (4) [24]

$$\lambda_{sl} = \frac{\bar{\lambda}_s^{\,2}}{b} \tag{4}$$

where $b$ is the mean width of the grinding scratches measured on the grinding surface and $\bar{\lambda}_s$ is a technical index of the abrasive wheel obtained by statistical analysis of the grinding wheel surface topography.

In Fig. 6, the contour of the grinding wheel is defined as circle $\odot W$, and $\widehat{OPB}$ is a micro arc on $\odot W$ near the coordinate origin. The circle equation is expressed in the following equation:

$$x^2 + \left(y - \frac{d_s}{2}\right)^2 = \left(\frac{d_s}{2}\right)^2 \tag{5}$$

According to the theory of curvature, a parabola has an osculating circle at the vertex with the same curvature radius. The center of the osculating circle is located on the double extension of the parabola vertex and focus. The parabola equation of circle $\odot W$ is defined in the following equation:

$$x^2 = d_s y \tag{6}$$

By inserting Eq. (6) into Eq. (3), the penetration depth can be expressed in Eqs. (7) and (8):

$$h(x) = \frac{2\lambda_{sl} v_w}{v_s} x = c_1 x \tag{7}$$

$$c_1 = 2\lambda_{sl} v_w / v_s \tag{8}$$

**2.2 Total Frictional Heat Flux Based on Single Grains.** Ohbuchi and Matsuo [25] measured the cutting force in single-grit orthogonal cutting process with both cubic boron nitride and diamond grains, and found that both the cutting force and the thrust force increased linearly with cutting depth. The thrust force can be expressed in the following equation:

$$F_t(x) = c_2 h(x) \tag{9}$$

For the grain, regardless of the material deformation in any of the three stages, the work done by friction can be considered as the product of force and speed. Each grain is a single-point heat source with its frictional work shown in the following equation:

$$W_i(x) = F_t(x_i) v_s = c_1 c_2 v_s x_i \tag{10}$$

where $x_i$ is the x-coordinate of the $\underline{i\text{th}}$ point $P(x_i, y_i)$.

For the whole contact surface $\widehat{OB}$, at any given moment, the total frictional work is the sum of the point heat work, as shown in the following equation:

$$W = \sum_{i=0}^{N} c_1 c_2 v_s x_i \tag{11}$$

Hundreds of active grains simultaneously participate in the frictional work during the grinding process. Some of them are part of the sliding process, and others are plowing and cutting. Based on the definition of the Riemann integral, the limitation sum of a discrete distributed point heat source can be expressed as the following equation:

$$W \approx \lim_{N\to\infty} \sum_{i=0}^{N} c_1 c_2 v_s x_i = \frac{N}{A} \int\int_o^B c_1 c_2 v_s x dA \tag{12}$$

where $A$ is the total area of the contact surface within the grinding zone, and $N$ is the total number of grains. $\gamma$ is the distribution density of grain obtained by$\gamma = N/A$, which represents the grain quantity in a unit area.

An equivalent continuously distributed surface heat source is proposed in the following equation for statistical modeling:

$$W = \int\int_O^B q_0(x) dA \tag{13}$$

where $q_0(x)$ is the thermal flux at point $P(x, y)$, and d$A$ is the area of a micro element. The integral domain is the complete grinding zone.

Based on Eqs. (11)–(13), the total surface heat flux created by grinding friction has two expressions.

$$\int\int_O^B \gamma c_1 c_2 v_s x dA = \int\int_O^B q_0(x) dA \tag{14}$$

Equation (14) represents the statistical frictional work on the total contact surface $\widehat{OB}$, but the equation is applicable for any part of the contact surface. For surface $\widehat{OP}$, it can be expressed by the following equation:

$$\int\int_0^x \gamma c_1 c_2 v_s x dA = \int\int_0^x q_0(x) dA \tag{15}$$

By taking the derivative of both sides, the statistical continuous heat flux can be written as the following equation:

$$q_0(x) = \gamma c_1 c_2 v_s x \tag{16}$$

**2.3 Heat Distribution Ratio Between a Grain and the Workpiece.** The heat distribution ratio is defined as the ratio of heat going into the workpiece to the total grinding heat

$$\epsilon = \frac{q_w}{q_0} = \frac{q_w}{q_g + q_w} \tag{17}$$

where $\epsilon$ is the heat distribution ratio; $q_w$ is the heat flux into the workpiece, including undeformed chips; $q_g$ is the heat flux into the grain; and $q_0$ is the total heat flux due to friction.

Outwater and Shaw [26] considered that heat was generated at three sources: (i) the grain wear flat workpiece interface; (ii) the chip shear plane; and (iii) the grain chip interface. Hahn [27] found that the third component is negligible compared to (i) and (ii). According to Hahn's theory, the whole friction heat had two flow directions: grains and workpiece; the heat distribution ratio is given by the following equation:

$$\epsilon = \left(1 + \frac{\lambda_g}{\sqrt{r_0 v_s (\lambda\rho C_p)_w}}\right)^{-1} \tag{18}$$

where the subscript $g$ is for grain, $w$ is for workpiece, $\lambda$ is the thermal conductivity, $r_0$ is the equivalent radius of the grain tip, $\rho$ is the density, and $C_p$ is the specific heat capacity.

Although Hahn neglected the third part of heat source, Eq. (18) still puts the second and third parts together in calculation. Heat flowing $(q_w)$ into the workpiece contains two portions: one part flows into the grinded workpiece (net heat into workpiece $q_n$) and the other part flows into undeformed chip (heat into chip $q_c$). Therefore, the sum of heat flowing into the workpiece can be expressed in the following equation:

$$q_w = \epsilon\gamma c_1 c_2 v_s x \tag{19}$$

**2.4 Heat Dissipation by Grinding Chips.** A portion of the heat is removed from the workpiece through chip removal. In Fig. 6, the red shaded micro block near point $P(x, y)$ is an undeformed chip. The heat energy $dQ_c$ inside the micro block is lost with the removal of the chip and can be expressed by the following equation:

$$dQ_c(x) = C_p(T) \cdot \rho_w \cdot B \cdot h(x) \cdot dx \cdot dT \tag{20}$$

where $C_p(T)$ is the specific heat capacity under constant pressure, which can be calculated by Equation (1); $B$ is the workpiece width; $T(x)$ is the temperature at point $P$; and $T_0$ is the ambient temperature. The energy flux lost by the chip is given by the following equation:

$$q_c(x) = \frac{-dQ}{B \cdot dx \cdot dt} = -C_p[T(x)] \cdot \rho_w \cdot \dot{T}(x) \cdot h(x) \tag{21}$$

By inserting Eq. (7) into Eq. (21), the heat flux $q_c$ can be expressed as the following equation:

$$q_c(x) = -c_1 \cdot C_p(T(x)) \cdot \rho_w \cdot \dot{T}(x) \cdot x > 0 \tag{22}$$

For the undeformed chip, its upper surface is the grinding touching zone. On the coordinate system in Fig. 6, point $A$ has the maximum workpiece surface temperature, which can be calculated by the Jaeger formula [2] given in Eq. (23) [28]

$$T_{\max} = T(x=0) = 2\bar{q}_w \sqrt{\frac{l}{\pi(\lambda\rho\bar{C}_p)_w v_w}} \tag{23}$$

$$l = \sqrt{a_p d_s} \tag{24}$$

$$T(x=l) = T_0 \tag{25}$$

where $\bar{q}_w$ is the average grinding heat flux, which can be calculated as $\bar{q}_w = q_w(l/2) = (1/2)\epsilon\gamma c_1 c_2 v_s l$, where $l$ is the length of the grinding contact arc and $\bar{C}_p$ is the average specific heat capacity of the workpiece. The maximum temperature $T_{\max}$ occurs at point $O$, and the temperature at point $C$ can be regarded as the ambient temperature $T_o$.

To obtain the derivative of the grinding temperature along the contact arc with respect to time ($\dot{T}$), an assumption is proposed that the temperature along contact arc $\widehat{OPB}$ can be considered as a linear distribution, as shown in Eq. (26). $\dot{T}(x)$ can be deduced by taking the derivative with respect to temperature $T(x)$

$$T(x) = -\frac{T_{\max} - T_0}{\sqrt{a_p d_s}} x + T_{\max}, \quad (0 \le x \le l) \tag{26}$$

$$\dot{T}(x) = -\frac{T_{\max} - T_0}{\sqrt{a_p d_s}} v_s \tag{27}$$

By inserting Eqs. (26) and (27) into Eq. (22), the heat flux removed by a chip is given by Eq. (28)

$$q_c(x) = c_3 \cdot C_p(T(x)) \cdot x \tag{28}$$

$$c_3 = \frac{c_1 \cdot \rho_w \cdot v_s \cdot (T_{\max} - T_0)}{\sqrt{a_p d_s}} \tag{29}$$

**2.5 Expression of the Equivalent Net Heat Flux.** Based on Eq. (2), the net heat flux into the workpiece is the remaining portion of the total workpiece heat flux. By inserting Eqs. (19) and (28) into Eq. (30), the expression of the net heat flux can be written in Equations (30) and (31)

$$q_n = q_w - q_c \tag{30}$$

$$q_n(x) = \epsilon\gamma c_1 c_2 v_s x - c_3 \cdot C_p\left(-\frac{T_{\max} - T_0}{\sqrt{a_p d_s}} x + T_{\max}\right) \cdot x \tag{31}$$

The specific heat capacity $C_p$ of most solid metals has a linear relationship with temperature as expressed in the following equation:

$$C_p(T) = k_0 + k_1 T \tag{32}$$

By combining Eqs. (31) and (32), the net heat flux can be expressed in Eq. (33). Therefore, the heat flux is a quadratic function of temperature without a constant term

$$q_n(x) = A_1 x + A_2 x^2, \quad (0 \le x \le l) \tag{33}$$

$$A_1 = \epsilon\gamma c_1 c_2 v_s - c_3(k_0 + k_1 T_{\max}) \tag{34}$$

$$A_2 = \frac{k_1 c_3 (T_{\max} - T_0)}{\sqrt{a_p d_s}} \tag{35}$$

## 3 Parameter Determination of the model

**3.1 Parameters of the Abrasive Wheel.** A white light interferometer (Talysurf PGI 1230, manufactured by Taylor Hobson) was used to scan the surface of an alumina abrasive wheel (WA400 × 30 ×27A80L5V35). The surface micro-topography of the wheel is shown in Fig. 7. The two-dimensional (2D) fast Fourier transform method was used to process the image data. The set of statistical parameters of a grain in Table 1 was obtained by using the statistic method given by Yan et al. [29]. Grains with irregular shapes are equivalent to ball-end cones. The average taper angle $\alpha$ is 85.6 deg. The equivalent radius $r_o$ of the grain tip is approximately 34.5 $\mu$m. The distribution density is approximately 4.56 $\text{mm}^{-2}$, and the mean scattered spacing $\bar{\lambda}_s$ is 0.470 mm.

**3.2 Parameters of the Material Properties.** The specific heat capacity of an alumina grain can be regarded as a constant (880 $\text{J}/(\text{kg}\cdot\text{K})$), and the density of alumina is 395 $\text{kg/m}^3$, as shown in Table 2.

For 2Cr12Ni4Mo3VNbN steel, as shown in Fig. 8, the specific heat capacity $C_p(T)$ can be represented as a linear function of temperature, as shown in Eq. (32), with $k_0 = 368.2\ \text{J}/(\text{kg}\cdot\text{K})$ and $k_1 = 0.7050\ \text{J}/(\text{kg}\cdot\text{C}^2)$. The density of this type of steel is 775 $\text{kg/m}^3$.

**3.3 Parameters of the Single Grain Cutting Process.** Single grain cutting test was conducted on a high-precision NC lathe, and the cutting forces were measured with a Kistler 5080A. As shown in Fig. 9, the workpiece was a thin-walled cylinder with a diameter of 200 mm. A single-point diamond was fixed on a MiniDyn 9265C2 force sensor, and the tangential forces associated with the cutting depth and cutting speed were acquired by the Kistler measurement system, as presented in Fig. 10, which shows that the tangential force was proportional to the cutting depth under different cutting speeds. The linear fitting equations are expressed in Eq. (36), where the cutting depth was measured in meters and force was measured in Newton

$$F_t = \begin{cases} 0.7422 \times 10^6 H, & v_s = 10\ \text{m/s} \\ 1.0697 \times 10^6 H, & v_s = 15\ \text{m/s} \\ 1.6918 \times 10^6 H, & v_s = 20\ \text{m/s} \end{cases} \tag{36}$$

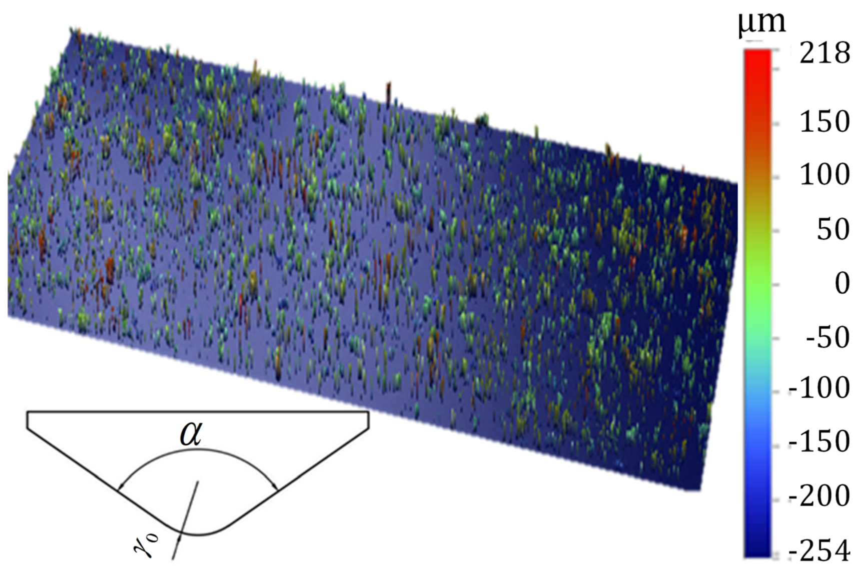


**Fig. 7 Surface microtopography of an alumina abrasive wheel**

**Table 1 Statistical parameters of alumina abrasive grains**

| $\alpha$/(deg) | $r_0$/($\mu$m) | $\gamma$/(mm$^{-2}$) | $\bar{\lambda}_s$/(mm) |
|---|---|---|---|
| 85.6 | 26.8 | 4.56 | 0.470 |

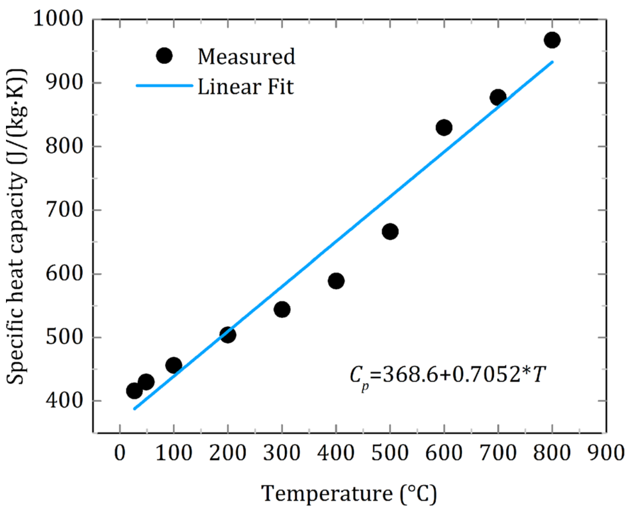


**Fig. 8 Specific heat of 2Cr12Ni4Mo3VNbN steel**

## 4 Simulation and Results

The net heat flux distribution was used as the moving heat source on the workpiece. A two-dimensional heat transfer model was built in ABAQUS with its subroutines, and the temperature field was computed. Then, the temperature–time curves were extracted for the subsequent experimental validation.

**4.1 Mathematical Expression of the Net Heat Flux.** The parameters are listed in Table 3 for a grinding depth of $a_p = 100\ \mu$m, wheel linear speed of $v_s = 20$ m/s, and workpiece feed speed of $v_w = 300$ mm/min. The equations of the heat flux are given as follows: The net heat flux in Eq. (39) was plugged into the FEM model as the heat source

$$q_o(x) = 4.24E^9 x, \quad (0 \le x \le l) \tag{37}$$

$$q_w(x) = 3.84E^9 x, \quad (0 \le x \le l) \tag{38}$$

$$q_n(x) = 2.51E^9 x + 1.51E^{11} x^2, \quad (0 \le x \le l) \tag{39}$$

Figure 11 shows all the heat flux curves distributed along the grinding contact arc. The net heat flux entering the workpiece is not a rectangle [30], triangle [1], or trapezoid, but a portion of a parabola.

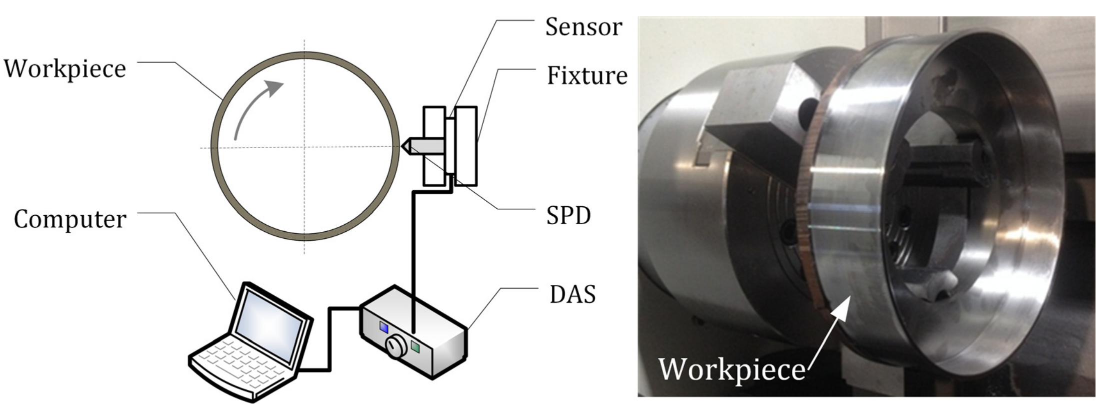


**Fig. 9 Schematic and appliance of single grain cutting**

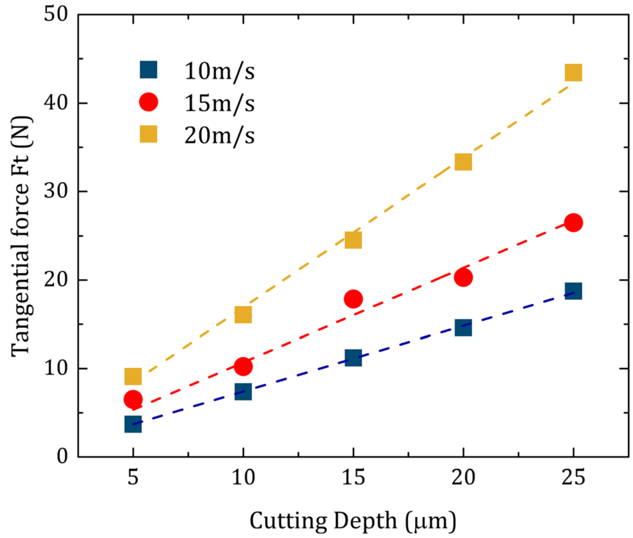


**Fig. 10 Tangential forces of single grain cutting**

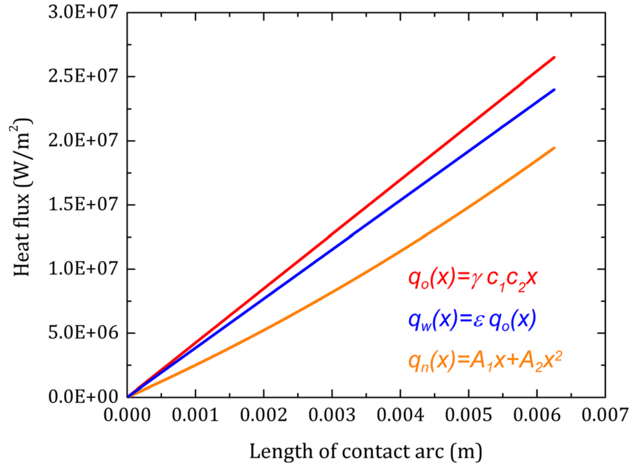


**Fig. 11 Heat flux distributions along the grinding contact arc. $a_p = 100\,\mu$m, $v_s = 20$ m/s and $v_w = 300$ mm/min.**

**Table 2 Thermophysical parameters of 2Cr12Ni4Mo3VNbN steel and alumina grain**

| Material | $\bar{C}_p/(\mathrm{J/(kg\cdot K)})$ | $\rho/(\mathrm{kg/m^3})$ | $\lambda/(\mathrm{W/(m\cdot K)})$ |
|---|---|---|---|
| Alumina grain | 520 | 396 | 30 |
| 2Cr12Ni4Mo3VNbN | 870 | 775 | 17 |

**Table 4 HTC of the grinding medium (unit: W/m² · K)**

| Type | Nongrinding zone | Grinding zone | |
|---|---|---|---|
| Dry | 10.45 | | $10.45 - v_s + 10\,v_s^{0.5}$ |
| Wet | $2.0\,E^3 \sim 1.2\,E^4$ | $2.9\,E^5$ | $(a_p \le 100\,\mu\mathrm{m},\ v_s = 20\,\mathrm{m/s})$ |
| | | $5.1\,E^4$ | $(a_p \ge 300\,\mu\mathrm{m},\ v_s = 20\mathrm{m/s})$ |

**Table 3 Parameters in the heat source model**

| Parameter | Value (SI) | Annotation |
|---|---|---|
| $a_p$ | $1.0\,E^{-4}$ m | |
| $A_1$ | $2.51\,E^9$ | By Eq. (34) |
| $A_2$ | $1.51\,E^{11}$ | By Eq. (35) |
| $b$ | $4.016\,E^{-4}$ m | |
| $c_1$ | $2.75\,E^{-5}$ | By Eq. (8) |
| $c_2$ | $1.69\,E^6$ N/m | By Eq. (36) |
| $c_3$ | $9.55\,E^5$ | By Eq. (29) |
| $\bar{C}_p$ | 870 J/(kg · K) | |
| $d_s$ | 0.4 m | |
| $l$ | $6.325\,E^{-3}$ m | By Eq. (24) |
| $r_0$ | $3.48\,E^{-5}$ m | |
| $T_{\max}$ | 1164 °C | By Eq. (23) |
| $v_s$ | 20 m/s | |
| $v_w$ | $5.0\,E^{-3}$ m/s | |
| $\gamma$ | $4.56\,E^6$ m$^{-2}$ | |
| $\epsilon$ | 0.904 | By Eq. (18) |
| $\lambda_g$ | 30 W/(m · K) | |
| $\bar{\lambda}_s$ | $4.70\,E^{-3}$ m | |
| $\lambda_{sl}$ | $5.50\,E^{-2}$ m | By Eq. (4) |
| $\rho_w$ | $7.75\,E^3$kg/m$^3$ | |

**4.2 Thermal Boundary Conditions.** Heat convection between the workpiece and the fluid medium is main energy transfer method during grinding. In wet grinding, abundant heat is removed by the grinding coolant in a process that is often called forced convection. However, in dry grinding, heat dissipates slowly into the air via free convection. Newton's law of cooling is used to quantitatively describe the heat flux of convection, as shown in the following equation:

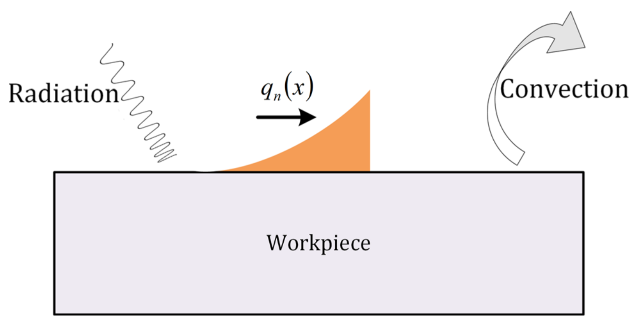


**Fig. 12 Thermal boundary conditions**

$$q = h(T - T_o) \tag{40}$$

Heat transfer coefficient $h$ has a strong influence on the temperature calculation. For dry grinding, no coolant is used, and HTC is the transfer coefficient of free air. For wet grinding, a coolant lubricant emulsion is used. The coolant is accelerated by the high-speed spinning abrasive wheel within the grinding contact area, and the HTC of the contact surface is larger than that of the noncontact surface. The HTC under different grinding conditions is listed in Table 4 according to related research [23,31–35].

Figure 12 shows the thermal boundary conditions of the FEM model. Based on the 2D model, a moving heat flux is applied to the upper surface, and both radiation and convection effects are considered.

**4.3 Simulation Results.** The temperature fields of the workpiece during wet and dry grinding for $a_p = 100\ \mu$m, $v_s = 20$ m/s, and $v_w = 300$ mm/min are shown in Fig. 13. The maximum temperature (approximately 1051 °C for dry grinding and 84 °C for wet grinding) occurs at the grinding contact surface. The coolant substantially lowers the grinding temperature via forced

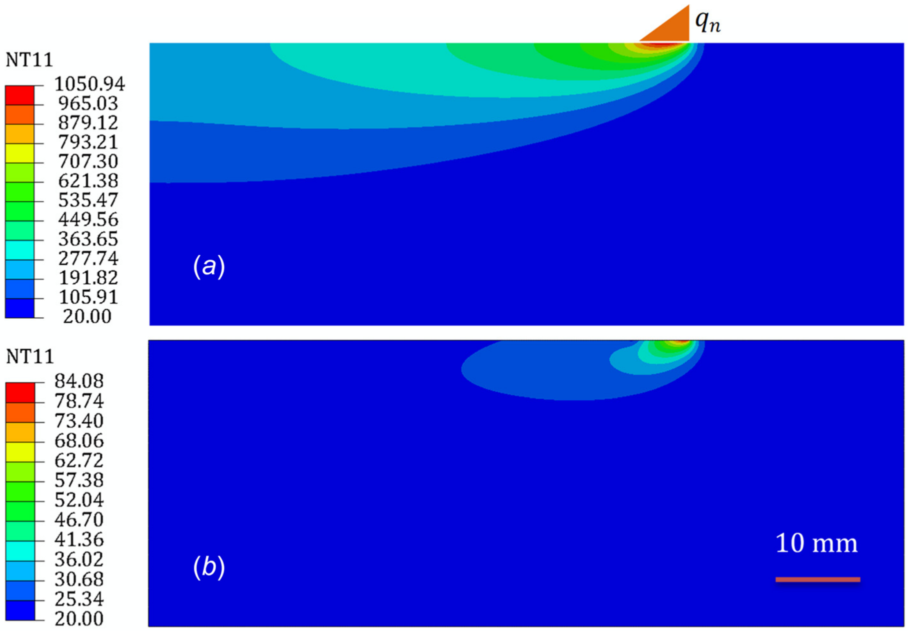


**Fig. 13 Temperature fields computed by FEM (unit: °C). $a_p = 100\,\mu$m, $v_s = 20$ m/s and $v_w = 300$ mm/min, dry grinding (*a*), wet grinding (*b*).**

**Table 5 Chemical composition of 2Cr12Ni4Mo3VNbN steel (wt %)**

| C | Cr | Ni | Mo | Nb | V | N | Fe |
|---|---|---|---|---|---|---|---|
| 0.02% | 12.09% | 3.46% | 3.80% | 0.38% | 0.47% | 1.43% | Balance |

**Table 6 Mechanical properties of 2Cr12Ni4Mo3VNbN steel**

| $\sigma_b$ (MPa) | $\sigma_s$ (MPa) | $\Psi$ | $\delta$ | $HB$ |
|---|---|---|---|---|
| ≥1350 | ≥1050 | ≥15% | ≥15% | >400 |

convection. Dry grinding is harmful to the workpiece as the temperature exceeds the phase transformation point of steel.

## 5 Measurement and Validation of the Grinding Temperature

**5.1 Workpiece Material Properties.** 2Cr12Ni4Mo3VNbN steel, a martensitic stainless steel widely used in steam turbine blades due to its excellent corrosion resistance, was used in the grinding experiment. Table 5 shows the chemical composition of the steel in percent weight [36], and the mechanical properties are given in Table 6.

As shown in Fig. 14, the microstructure of tempered steel is a ferrite matrix with fine spherical carbide. The supersaturated carbon dissolves to form carbides with metal elements. Tempered steel is a stable structure with excellent mechanical properties.

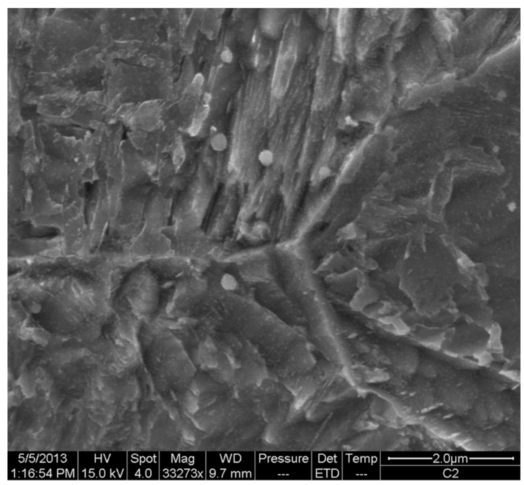


**Fig. 14 SEM micrograph of tempered 2Cr12Ni4Mo3VNbN steel**

### 5.2 Measurement System for the Grinding Process

*5.2.1 Infrared Measurement Theory and In Situ Device.* All matter with a temperature above absolute zero emits electromagnetic radiation. The radiant flux can be calculated via the Stefan–Boltzmann law expressed in Eq. (41). An infrared sensor can measure the magnitude of the radiant flux $q$. After the emissivity $\varepsilon$ is determined, the temperature $T$ can be obtained

$$q = \varepsilon\sigma\left(T^4 - T_0^4\right) \tag{41}$$

The in situ infrared measurement system shown in Fig. 15 was used to determine the temperature field. A cylindrical workpiece with a blind hole on the bottom and a 1 mm thick layer for grinding was manufactured using 2Cr12Ni4Mo3VNbN steel. The workpiece was embedded into a fixture, which was installed on a workbench. Two infrared sensors (M-2H and M-3L) were used to capture the infrared light emitted from the blind hole. The technical parameters of the two infrared sensors are listed in Table 7. The selection between the two sensors depended on the maximum grinding temperature and measurement range. The sensor was fixed on a precision cross table, and the focal point was precisely focused on the bottom of the blind hole by adjusting the position of the sensor. In the initial state, the gauging point (focal point of the sensor) was located under the grinding plane, with a depth of one millimeter. As the grinding went on layer by layer, the depth from gauging point to grinding plane would reduce a thin one-layer thickness for each grinding pass. Therefore, the temperature curves of varying depth under the grinding plane were obtained.

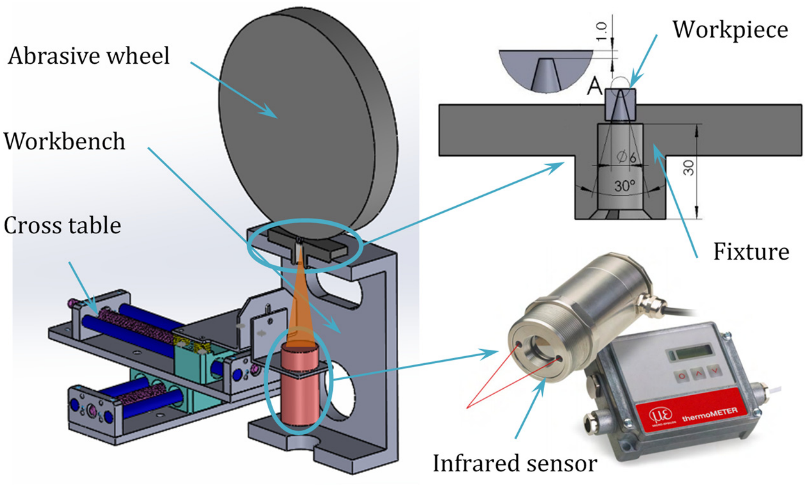


**Fig. 15 Schematic sketch of the infrared measurement system**

**Table 7 Technical parameters of the M-2H infrared sensor**

| Sensor | Range (°C) | Sample frequency/(Hz) | Temperature resolution/(°C) | Spatial resolution/(mm) |
|---|---|---|---|---|
| M-2H | 385–1600 | 1000 | 0.2 | 0.5 |
| M-3 L | 50–375 | | | |

As shown in Fig. 16, the measurement workbench was placed on the grinding machine table, and the abrasive wheel was used to grind the upper surface of the workpiece. The temperature signal was collected by the infrared sensor and was recorded by a computer. According to our previous work [37], the emissivity is close to 1 (approximately 0.98), and the blind hole under the workpiece can be regarded as an ideal black body.

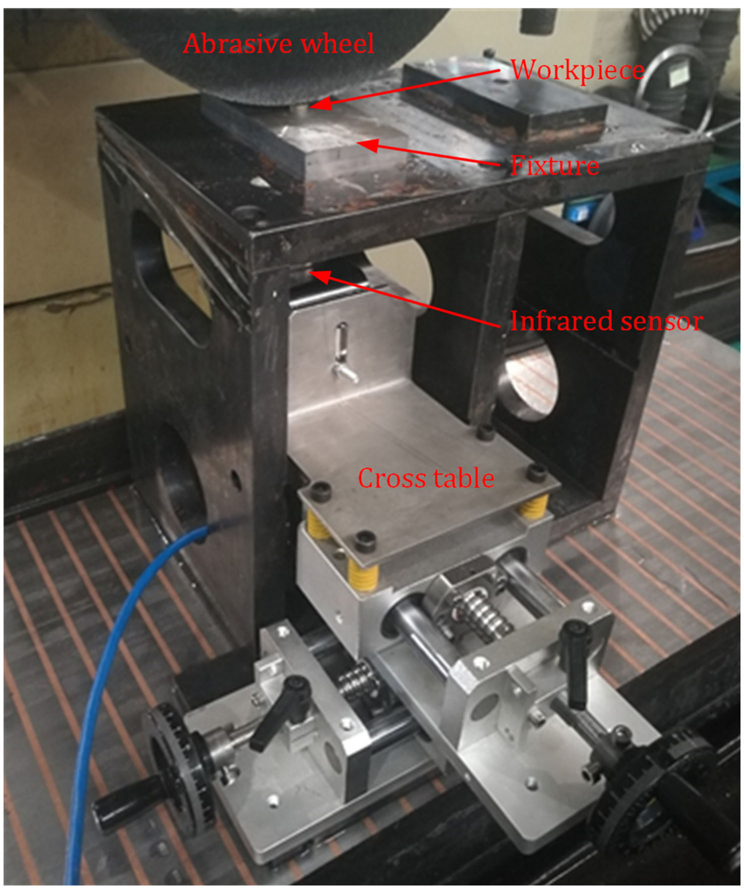


**Fig. 16 The infrared measurement system placed on a grinding machine table**

Table 8 Processing parameters of the grinding tests

| $a_p$ ($\mu$m) | $v_w$ (mm/min) | $v_s$ (m/s) | Grinding fluid |
|---|---|---|---|
| 30, 50, 100, 300 | 300 | 10, 20 | Dry, Wet |

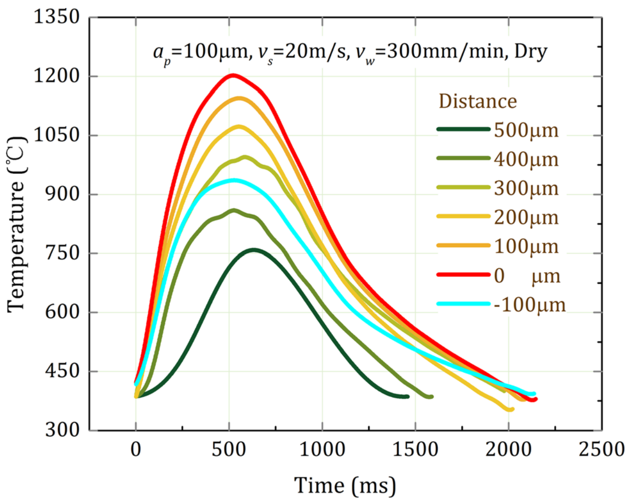


**Fig. 17 Grinding temperature variation curves**

*5.2.2 Experimental Scheme.* Grinding tests were conducted on a Schleifring BLOHM Planmat HP408 precision grinding machine. An alumina abrasive wheel (WA400 × 30 ×27A80L5V35) was used. Table 8 summarizes the grinding processing parameters. In a layer-by-layer grinding process with a fixed grinding depth $a_p$, the workpiece should be cooled to the ambient temperature after one grinding pass. Both dry and wet grinding tests were conducted in the experiment. During the wet grinding, coolant lubricant emulsion was sprayed to the workpiece in an effort to cool.

### 5.3 Experimental Results

*5.3.1 Experimental Results of the Grinding Temperature.* As shown in Fig. 17, the measurement device acquired the grinding temperature variation curves at different depth. For each fixed feed pass, the grinding temperature initially increased and then decreased. As grinding pass increased layer by layer, the depth (the distance between gauging point and grinding plane) decreased from 500 $\mu$m to 0 $\mu$m, and the grinding temperature gradually increased. When the depth reduced to 0 $\mu$m, the blind hole would be worn out. At this time, the bottom of blind-hole (the gauging point) was exactly appearing on the grinding plane (the upper surface of the workpiece). As shown in Fig. 17, the maximum temperature was 1202 °C when the depth was zero; the temperature increased rapidly, at an average rate of 1000 °C/s, and decreased slowly, at an average rate of 200 °C/s. After the blind hole being worn out, the temperature of the next grinding pass dropped rapidly; the temperature variation was shown in the curve with a depth of −100 $\mu$m.

The temperature field is a steady field at a constant feed speed in two-dimensional space. The temperature–time curves can be transformed into the temperature field, as shown in Fig. 18. The maximum temperature point is located in the grinding contact zone, and the vertical temperature gradient can reach 500 °C/mm.

*5.3.2 Maximum Grinding Temperature.* Figure 19 shows the maximum grinding temperature. During dry grinding, the grinding temperature increased with the increasing grinding depth. The grinding temperature increased rapidly when the grinding depth was less than 100 $\mu$m; however, the maximum grinding

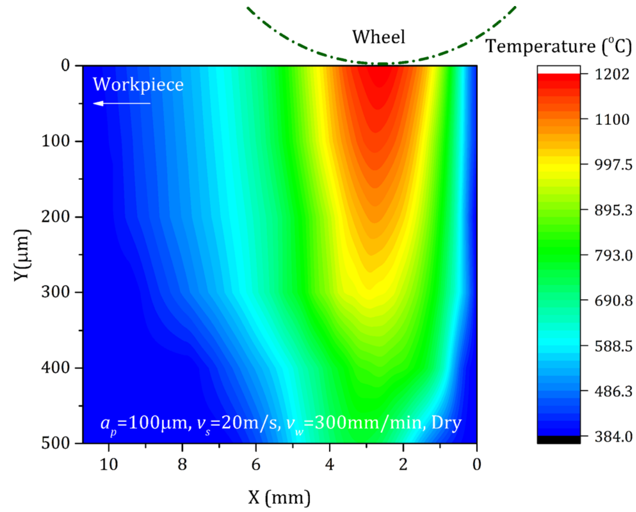


**Fig. 18 Experimentally measured grinding temperature field (unit: °C)**

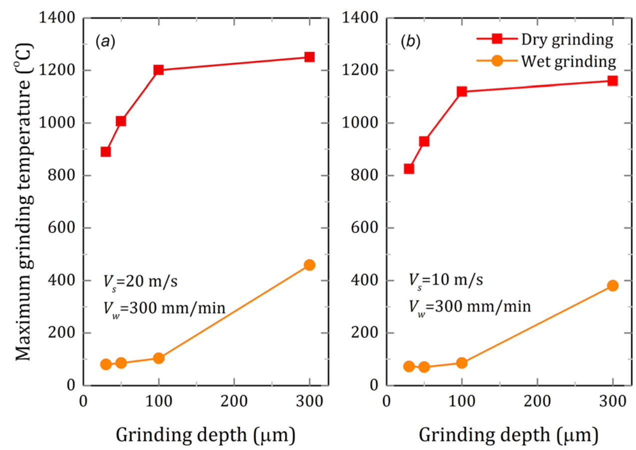


**Fig. 19 Maximum grinding temperature of the workpiece**

temperature increased slowly when the grinding depth was greater than 100 $\mu$m. As the grinding depth increased, the plastic deformation work and frictional force increased, and more consumed energy was converted to heat, which caused the temperature to increase. The coolant effectively decreased the grinding temperature through its forced convection effect.

## 6 Validation and Discussion

**6.1 Validation of the Temperature–Time Curves.** Two points of the workpiece were studied: one on the upper surface and the other 300 $\mu$m below the upper surface. Based on the simulated and experimental temperature fields, respectively, represented in Figs. 13 and 18, the temperature–time curves are compared separately in Fig. 20. During the increasing temperature period, the simulated curves coincided with the experimental curves; however, during the decreasing temperature period, the experimental temperature decreased faster than the simulated temperature. The reason for the difference may be the structure of the workpiece used in the experiment. The cavity under the workpiece damaged the integrality of the structure, and convection and radiation effects made the temperature decline rapidly during the prolonged decreasing temperature period. The simulated and experimental curves have almost identical peak temperatures. The relative errors are less than 10% for both points.

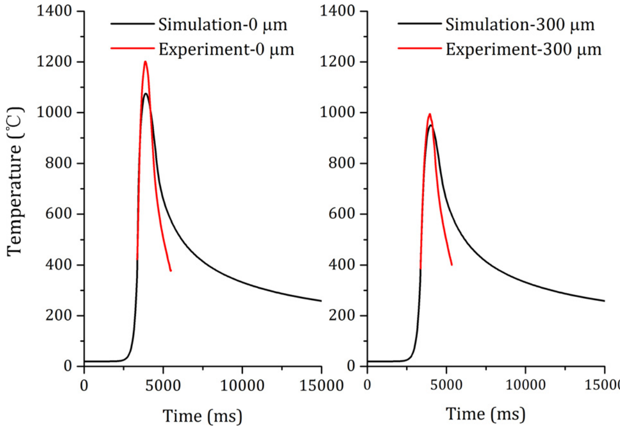


**Fig. 20 Comparison of the simulated and experimental temperature–time curves. $v_s = 20$ m/s, $v_w = 300$ mm/min, dry grinding.**

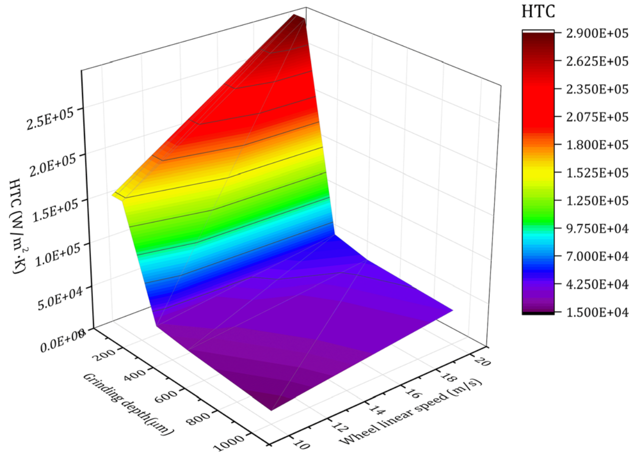


**Fig. 22 HTC of the grinding contact zone during normal grinding and creep feed grinding. $v_w = 300$ mm/min, wet grinding.**

**6.2 Validation of the Maximum Temperature.** A comparison of the maximum temperature on the upper surface for the simulated and experimental data is shown in Fig. 21. The two diagrams indicate that the simulation results corresponded with the experiment results, and the relative error was almost less than 20%. Considering parameter error and modeling error, the statistical model of the equivalent grinding heat source is sufficient to predict the grinding temperature field.

**6.3 HTC within Grinding Contact Area.** Table 4 shows that the HTC within the grinding contact zone underwent a large transition when the grinding depth exceeded 300 $\mu$m. Grinding with a grinding depth less than 100–200 $\mu$m is known as conventional grinding; otherwise, grinding is defined as creep feed grinding. Creep feed grinding is a grinding process with a large cutting depth and low feed speed. The cutting depth is usually 10–30 times that used in conventional grinding [2,38], and the feed speed is typically less than 60 mm/min [39]. The deeper grinding depth results in a larger material removal rate and higher productivity but generates extra heat, leading to increased temperature at both the workpiece and grinding wheel [40].

Due to large grinding depth and long contact length, it is difficult for coolant to penetrate the grinding zone during creep feed grinding. Even if coolant is used, the temperature of the grinding zone rises rapidly and reaches an elevated magnitude. As shown

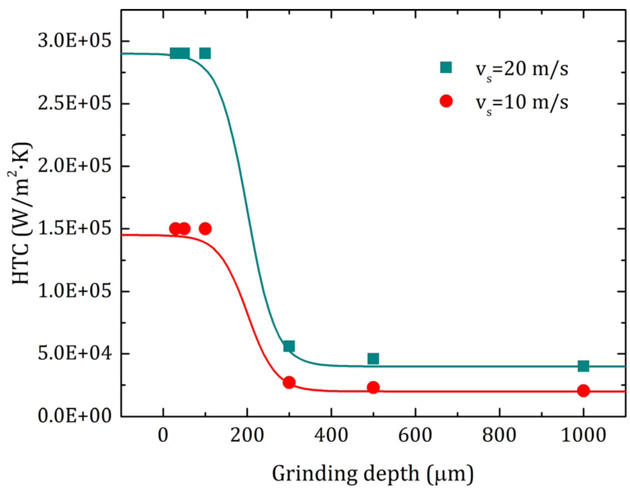


**Fig. 23 HTC fitting results. $v_w = 300$ mm/min, wet grinding.**

in Fig. 21, the maximum temperature can exceed 400 °C when the grinding depth is 300 $\mu$m.

Heat transfer coefficient is difficult to measure experimentally under all the different grinding parameters; therefore, an FEM-based inversed calculation method was adopted to calculate

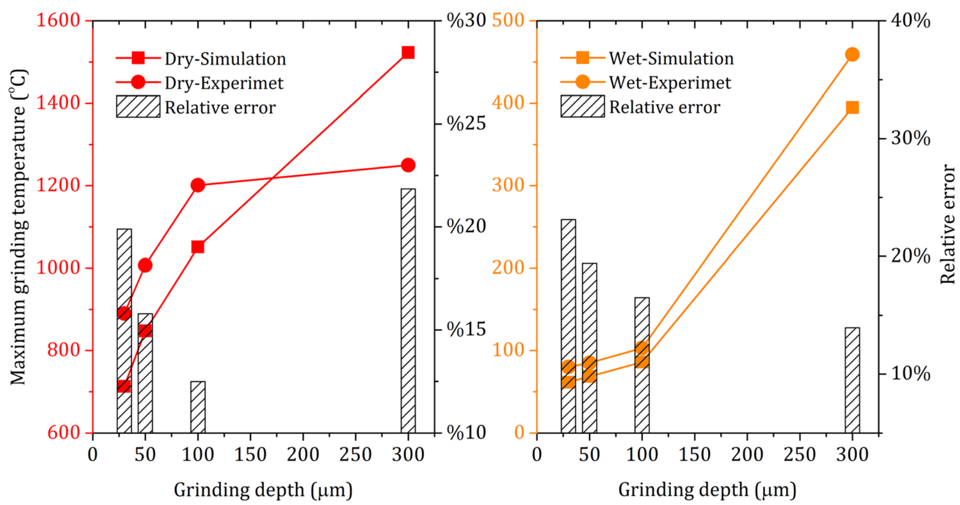


**Fig. 21 Comparison of the simulated and experimental maximum temperature. $v_s = 20$ m/s, $v_w = 300$ mm/min.**

the precise HTC in the grinding contact zone. With the goal of determining the experimental maximum grinding temperature, the HTC under different grinding process parameters can be obtained by the inversed calculation method [41,42]. All the tested and calculated HTC values are plotted in Fig. 22, and an empirical equation is proposed and fitted in Eq. (42). The equation accurately predicts the changes in HTC during both conventional grinding and creep feed grinding, as shown in Fig. 23. It can be seen that the HTC during creep feed grinding is significantly lower than that during conventional grinding

$$h = \left[2000 + \frac{12500}{(1 + 1.03^{a_p})}\right] v_s \tag{42}$$

where $a_p$ is the grinding depth in $\mu$m, $v_s$ is the wheel linear speed in m/s, and $h$ is the HTC in $\mathrm{W/m^2 \cdot K}$.

## 7 Conclusions

Based on the definition of the Riemann integral, the summation limit of the discrete point heat sources was transformed into the integral of a continuous function. A statistical heat flux model was proposed to predict the grinding temperature field. The mathematical derivation indicated that the net heat flux equation is a quadratic function of temperature.

Grinding temperature fields were measured using a specially designed in situ temperature measurement system, and the reliability and correctness of the statistical heat flux model were validated according to experimental temperature–time curves and the maximum grinding temperature. A comparison of the results demonstrated that the relative error between the simulated and experimental maximum temperature was less than 20%.

A FEM-based inversed calculation method was adopted to obtain the HTC. An empirical equation was proposed to predict the changes in HTC within the grinding contact zone. The fitting results indicated that the empirical equation can accurately describe the HTC variation for both conventional grinding and creep feed grinding.


## Funding Data

- National Security Major Basic Research Program of China (Grant No. 61328302).
- National Basic Research Program of China (Grant No. 2011CB013404).


## Nomenclature

$a_p$ = grinding depth of the abrasive wheel
$A$ = area of the grinding contact surface
$A_k$ = impact toughness
$A_1$ = monomial coefficient
$A_2$ = quadratic coefficient
$b$ = mean width of grinding scratches
$B$ = width of workpiece
$c_1$ = coefficient
$c_2$ = coefficient
$c_3$ = coefficient
$C_p$ = specific heat capacity
$\bar{C}_p$ = average specific heat capacity
$d_s$ = abrasive wheel diameter
$F_t$ = tangential cutting force of single grain cutting
$h$ = heat transfer coefficient
$H$ = cutting depth of single grain
$HB$ = brinell hardness
$k_0$ = coefficient
$k_1$ = coefficient
$l$ = length of the grinding contact arc
$N$ = total number of grains in the grinding contact surface
$P$ = radiant flux
$q_c$ = heat flux taken by chip
$q_g$ = heat flux going into grain
$q_n$ = net heat flux entering into workpiece
$q_w$ = heat flux entering into workpiece
$\bar{q}_w$ = average heat flux entering into workpiece
$q_0$ = total heat flux generated by friction
$Q_c$ = heat energy taken by chip
$r_0$ = equivalent radius of grain tip
$t$ = time
$T$ = temperature
$T_{\max}$ = maximum temperature of grinding zone
$T_0$ = ambient temperature
$v_{\mathrm{air}}$ = air flow rate
$v_s$ = wheel speed
$v_w$ = workpiece feed speed
$W$ = frictional work
$x$ = horizontal axis of grinding contact zone
$y$ = vertical axis of grinding contact zone
$\alpha$ = average taper angle of grain
$\gamma$ = distribution density of grain
$\delta$ = elongation
$\varepsilon$ = emissivity
$\epsilon$ = heat distribution ratio
$\lambda$ = thermal conductivity
$\lambda_g$ = thermal conductivity of grain
$\lambda_{sl}$ = average distance between two effective front and back grains
$\bar{\lambda}_s$ = mean scattered spacing of abrasive grain
$\rho$ = density of mass
$\sigma$ = Stefan–Boltzmann constant
$\sigma_b$ = tensile strength
$\sigma_s$ = yield strength
$\Psi$ = reduction of area

## References


[1] Lefebvre, A., Vieville, P., Lipinski, P., and Lescalier, C., 2006, "Numerical Analysis of Grinding Temperature Measurement by the Foil/Workpiece Thermocouple Method," Int. J. Mach. Tools Manuf., **46**(14), pp. 1716–1726.
[2] Jaeger, J. C., 1942, "Moving Sources of Heat and the Temperature of Sliding Contacts," J. Proc. R. Soc. New South Wales, **76**, pp. 203–224.
[3] Mamalis, A., Manolakos, D., Markopoulos, A., Kunádrk, J., and Gyáni, K., 2003, "Thermal Modelling of Surface Grinding Using Implicit Finite Element Techniques," Int. J. Adv. Manuf. Technol., **21**(12), pp. 929–934.
[4] Lefebvre, A., Lanzetta, F., Lipinski, P., and Torrance, A., 2012, "Measurement of Grinding Temperatures Using a Foil/Workpiece Thermocouple," Int. J. Mach. Tools Manuf., **58**, pp. 1–10.
[5] Rowe, W., Black, S., Mills, B., Qi, H., and Morgan, M., 1995, "Experimental Investigation of Heat Transfer in Grinding," CIRP Ann. Manuf. Technol., **44**(1), pp. 329–332.
[6] Liao, Y., Luo, S., and Yang, T., 2000, "A Thermal Model of the Wet Grinding Process," J. Mater. Process. Technol., **101**(1), pp. 137–145.
[7] Jiang, J., Ge, P., Sun, S., Wang, D., Wang, Y., and Yang, Y., 2016, "From the Microscopic Interaction Mechanism to the Grinding Temperature Field: An Integrated Modelling on the Grinding Process," Int. J. Mach. Tools Manuf., **110**, pp. 27–42.
[8] Dyakonov, A. A., 2014, "Simulated Stochastic Thermo-Physical Model of Grinding Process," World Congress on Engineering and Computer Science (WCECS), San Francisco, CA, Oct. 22–24, pp. 914–917.
[9] Rumford, B. C. O., 1798, "An Inquiry Concerning the Source of the Heat Which Is Excited by Friction. By Benjamin Count of Rumford, FRSMRIA," Philos. Trans. R. Soc. London Ser. I, **88**, pp. 80–102.
[10] Shore, H., 1924, *Tool and Chip Temperatures in Machine Shop Practice*, Massachusetts Institute of Technology, Cambridge, MA.
[11] Schwerd, F., 1933, "Determination of the Temperature Distribution During Cutting Z," VDI Z., **77**, pp. 211–216.
[12] Boothroyd, G., 1961, "Photographic Technique for the Determination of Metal Cutting Temperatures," Br. J. Appl. Phys., **12**(5), p. 238.
[13] Ueda, T., Hosokawa, A., and Yamamoto, A., 1986, "Measurement of Grinding Temperature Using Infrared Radiation Pyrometer With Optical Fiber," ASME J. Eng. Ind., **108**(4), pp. 247–251.
[14] Kato, T., and Fujii, H., 1997, "Temperature Measurement of Workpiece in Surface Grinding by PVD Film Method," ASME J. Manuf. Sci. Eng., **119**(4B), pp. 689–694.
[15] Yoshioka, H., Hashizume, H., and Shinn, H., 2004, "In-Process Microsensor for Ultraprecision Machining," IEEE Proc. Sci., Meas. Technol., **151**(2), pp. 121–125.
[16] Ueda, T., Hosokawa, A., and Yamamoto, A., 1985, "Studies on Temperature of Abrasive Grains in Grinding—Application of Infrared Radiation Pyrometer," ASME J. Manuf. Sci. Eng., **107**(2), pp. 127–133.

[17] Upadhyaya, R., and Malkin, S., 2004, “Thermal Aspects of Grinding With Electroplated CBN Wheels,” ASME J. Manuf. Sci. Eng., **126**(1), pp. 107–114.
[18] Li, Z., Ding, W., Shen, L., Xi, X., and Fu, Y., 2016, “Comparative Investigation on High-Speed Grinding of TiCp/Ti–6Al–4V Particulate Reinforced Titanium Matrix Composites With Single-Layer Electroplated and Brazed CBN Wheels,” Chin. J. Aeronaut., **29**(5), pp. 1414–1424.
[19] Chandrasekar, S., Farris, T., and Bhushan, B., 1990, “Grinding Temperatures for Magnetic Ceramics and Steel,” ASME J. Tribol., **112**(3), pp. 535–541.
[20] Kops, L., and Shaw, M. C., 1982, “Thermal Radiation in Surface Grinding,” CIRP Ann. Manuf. Technol., **31**(1), pp. 211–214.
[21] Xu, X., 2001, “Experimental Study on Temperatures and Energy Partition at the Diamond–Granite Interface in Grinding,” Tribol. Int., **34**(6), pp. 419–426.
[22] Hwang, J., Kompella, S., Chandrasekar, S., and Farris, T. N., 2003, “Measurement of Temperature Field in Surface Grinding Using Infra-Red (IR) Imaging System,” ASME J. Tribol., **125**(2), pp. 377–383.
[23] Jin, T., Stephenson, D., and Rowe, W., 2003, “Estimation of the Convection Heat Transfer Coefficient of Coolant Within the Grinding Zone,” Proc. Inst. Mech. Eng., Part B, **217**(3), pp. 397–407.
[24] Malkin, S. G. C., 2008, *Grinding Technology: Theory and Applications of Machining With Abrasives*, Industrial Press, South Norwalk, CT.
[25] Ohbuchi, Y., and Matsuo, T., 1991, “Force and Chip Formation in Single-Grit Orthogonal Cutting With Shaped CBN and Diamond Grains,” CIRP Ann. Manuf. Technol., **40**(1), pp. 327–330.
[26] Outwater, J., and Shaw, M., 1952, “Surface Temperatures in Grinding,” Trans. ASME, **74**(1), p. 73.
[27] Hahn, R. S., 1962, “On the Nature of the Grinding Process,” Third Machine Tool Design and Research Conference, Birmingham, UK, Sept. 24–28, pp. 129–154.
[28] Lavine, A., Malkin, S., and Jen, T., 1989, “Thermal Aspects of Grinding With CBN Wheels,” CIRP Ann. Manuf. Technol., **38**(1), pp. 557–560.
[29] Yan, L., Rong, Y., and Jiang, F., 2011, “Quantitative Evaluation and Modeling of Alumina Grinding Wheel Surface Topography,” Jixie Gongcheng Xuebao (Chin. J. Mech. Eng.), **47**(17), pp. 179–186.
[30] Parente, M. P. L., Jorge, R. M. N., Vieira, A. A., and Baptista, A. M., 2012, “Experimental and Numerical Study of the Temperature Field During Creep Feed Grinding,” Int. J. Adv. Manuf. Technol., **61**(1–4), pp. 127–134.
[31] Nie, Z., Wang, G., Lin, Y., and Rong, Y., 2015, “Precision Measurement and Modeling of Quenching-Tempering Distortion in Low-Alloy Steel Components With Internal Threads,” J. Mater. Eng. Perform., **24**(12), pp. 1–12.
[32] Bergman, T. L., 2011, *Introduction to Heat Transfer*, Wiley, Hoboken, NJ.
[33] Bergman, T. L., and Incropera, F. P., 2011, *Fundamentals of Heat and Mass Transfer*, Wiley, Hoboken, NJ.
[34] Khabari, A., Zenouzi, M., O’Connor, T., and Rodas, A., 2014, “Natural and Forced Convective Heat Transfer Analysis of Nanostructured Surface,” World Congress on Engineering (WCE), London, July 2–4.
[35] Lavine, A. S., 1988, “A Simple Model for Convective Cooling During the Grinding Process,” ASME J. Eng. Ind., **110**(1), pp. 1–6.
[36] Nie, Z., Wang, G., Yu, J., Liu, D., and Rong, Y., 2016, “Phase-Based Constitutive Modeling and Experimental Study for Dynamic Mechanical Behavior of Martensitic Stainless Steel Under High Strain Rate in a Thermal Cycle,” Mech. Mater., **101**, pp. 160–169.
[37] Liu, D., Wang, G., Nie, Z., and Rong, Y., 2016, “An In-Situ Infrared Temperature-Measurement Method With Back Focusing on Surface for Creep-Feed Grinding,” Measurement, **94**, pp. 645–652.
[38] Ichida, Y., 2001, “Creep Feed Profile Grinding of Ni-Based Superalloys With Ultrafine-Polycrystalline cBN Abrasive Grits,” Precision Eng., **25**(4), pp. 274–283.
[39] Grigoriev, S. N., Starkov, V. K., Gorin, N. A., Krajnik, P., and Kopac, J., 2014, “Creep-Feed Grinding: An Overview of Kinematics, Parameters and Effects on Process Efficiency,” Strojniški Vestnik-J. Mech. Eng., **60**(4), pp. 213–220.
[40] Kim, H.-J., Kim, N.-K., and Kwak, J.-S., 2006, “Heat Flux Distribution Model by Sequential Algorithm of Inverse Heat Transfer for Determining Workpiece Temperature in Creep Feed Grinding,” Int. J. Mach. Tools Manuf., **46**(15), pp. 2086–2093.
[41] Du, P., Wang, G., Nie, Z., and Rong, Y., 2014, “A FEM-Based Inverse Calculation Method for Determination of Heat Transfer Coefficient in Liquid Quenching Process,” TMS 143rd Annual Meeting & Exhibition, San Diego, CA, Feb. 16–20, p. 309.
[42] Lin, B., Morgan, M. N., Chen, X. W., and Wang, Y. K., 2009, “Study on the Convection Heat Transfer Coefficient of Coolant and the Maximum Temperature in the Grinding Process,” Int. J. Adv. Manuf. Technol., **42**(11), pp. 1175–1186.